

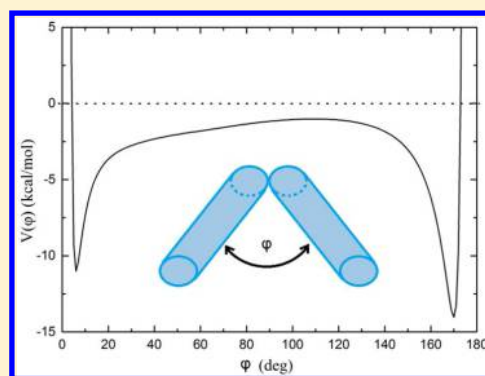
Molecular Dynamics Simulation for the Dynamics and Kinetics of Folding Peptides in the Gas Phase

Iraklis Litinas and Andreas D. Koutselos*

Department of Chemistry, Physical Chemistry Laboratory, National and Kapodistrian University of Athens, Panepistimiopolis, 15771 Athens, Greece

Supporting Information

ABSTRACT: The conformations of flexible molecular species, such as oligomers and oligopeptides, and their interconversion in the gas phase have been probed by ion mobility spectrometry measurements. The ion motion is interpreted through the calculation of effective cross sections in the case of stable conformations of the macromolecules. However, when the molecular structures transform to each other as the ions collide with gas atoms during their flight through the drift tube, the introduction of an average cross section is required. To provide a direct way for the reproduction of the ion motion, we employ a nonequilibrium molecular dynamics simulation method and consider a molecular model that consists of two connected stiff cylindrical bodies interacting through an intramolecular model potential. With this procedure we have calculated the ion mobility as a function of temperature for a prototype peptide that converts between a helical and an extended globular form. The results are in good agreement with ion mobility spectrometry data confirming that an angular vibration coordinate can be used for the interpretation of the shifting of the drift-time distributions at high temperatures. The approach produces mean kinetic energies as well as various combined distributions of the ion degrees of freedom. It is easily applied to flexible macromolecular ions and can be extended to include additional degrees of freedom.



INTRODUCTION

Macromolecular ions drifting in low density He gas under the action of a weak electric field in ion mobility spectrometry measurements may present a static or dynamic structural behavior depending on the gas temperature. It has been observed in sodiated oligomers^{1,2} and protonated oligopeptides,^{3,4} among other ionic molecular species, that at low temperature multiple relatively stable structures prevail as the ions transverse through the spectrometer, though at high temperatures some of these structures interchange within themselves throughout the ion flight.^{5–7} In the latter case the conformers of certain oligopeptides have been assumed to participate in a unimolecular reaction that involves a reaction coordinate associated with the structural change of the ion. Although this dynamical behavior emerges through excitation of various molecular modes and follows a cascade of structural processes, one bending mode has been considered dominant. This assumption appears adequate for the interpretation of the experimental mobility measurements and the characterization of the equilibrated properties of the processes. From the experimental transport cross sections and their temperature dependence various equilibrium constants have been obtained together with the enthalpy and entropy of activation of the folding processes.⁷ An additional factor that interferes with the ion transport properties is the position of the charge on the peptides, which may transfer between different sites as the structure of the peptides changes. The coil–helix transitions of

various designed peptides have been associated with charge transfer between bending or end sites that stabilizes the peptide structures.^{5,8} Such charge shifts change the point of application of the external electric field and may introduce dynamic effects in the ion internal motion.

The interpretation of ion mobility spectrometry measurements rests on the expression that connects the ion–He cross section Ω to the experimental ion drift velocity v_d through the mobility $K = v_d/E$ at weak electric field strength E . The expression has been obtained, among other more general ways, through a two temperature kinetic theory solution at low approximation⁹

$$K = \frac{3Ze}{16N} \left(\frac{2\pi}{\mu k T_{\text{eff}}} \right)^{1/2} \frac{1}{\Omega^{1,1}} \quad (1)$$

where Z is the charge of the ion, N is the gas number density, and μ is the reduced ion–neutral mass. The effective temperature T_{eff} of the ions at weak fields is approximated well through the Wannier formula¹⁰

$$\frac{3}{2} k T_{\text{eff}} = \frac{3}{2} k T_w \equiv \frac{3}{2} k T + \frac{1}{2} M v_d^2 \quad (2)$$

Received: June 1, 2015

Revised: November 15, 2015

Published: December 7, 2015

Here, M and T are the atomic mass and temperature of the gas, respectively, and T_w is the Wannier temperature. At relatively high temperatures (and weak electric fields) T_{eff} is well approximated by T . In general, the momentum transfer collision integral $\Omega^{1,1}$ is approximated by Ω , which is the ion–atom cross section averaged over all orientations. In most cases Ω is calculated through consideration of a rigid molecular frame,^{1,11,12} though the effect of rotation and vibration in small molecular ions has also been examined.^{13,14} The interpretation of the dependence of the ion mobility spectrometry measurements on temperature for flexible peptide ions in He has been confirmed indirectly by molecular simulations.⁷ The relatively stable conformations have been determined first through molecular dynamics simulations with an effective annealing procedure and consequently their ion–atom cross sections have been calculated through a scattering method employing model interaction potentials. A direct reproduction of the peptide conformation dynamics through MD simulations has not been pursued due to difficulties in following the trajectory of the many peptide degrees of freedom at the atomistic level.

To study directly the conformation dynamics of flexible peptides or macromolecules and its relation with the rotational and translational motion, we employ a nonequilibrium molecular dynamics (MD) simulation method to simulate the ion motion¹⁵ through the use of a molecular model with simplified structure, giving emphasis to the bending vibration. The performance of the method and the simplified structure model is examined through the reproduction of the ion mobility spectrometry data for a flexible designed peptide. The MD method has been used in the past mostly for the reproduction of the transport and dynamics of small ions in gases under the action of an electrostatic field.^{16–19}

Experiments have shown that the increase of the buffer gas temperature in drift tubes modifies the drift-time distributions of ion conformers.^{2,6,7} At low temperature in certain cases a number of peaks appear in the distribution that have been ascribed to relatively stable peptide conformations. As the temperature is raised, two main modifications appear in the experimental time distributions. The first one involves the disappearance of certain peaks attributed to thermal destabilization of relevant conformations and their transformation to the remaining more stable ones. The second modification involves the shift of peaks with temperature from values characterizing one conformer to values of another. The explanation of this variation has been based on the possibility conformations to interconvert to one another during their drift-tube flight. The relative residence time of the peptide spent on distinct structures has been considered to weigh the contribution of the conformers cross sections on the measured mean cross section. As the temperature increases, the initial contribution of the more stable structure is replaced gradually by one that corresponds to a structure which is populated at high temperatures.

On the basis of a two-state polymer folding model,²⁰ we consider the peptide to consist of two stiff helical parts represented by hollow cylindrical bodies connected at a point of their rim. Locally stable conformation with respect to the angle between the two rigid parts, φ , are introduced through consideration of an intramolecular potential, $V(\varphi)$, that depends on φ . We consider here two competing conformations with a closed (globule) and an extended (helix) form and introduce two minima in the potential, one at a small angle and one close to π . Thus, the peptide is allowed to move under the

action of the electric field and accumulate translational, rotational and angular-vibration energy though the collisions with the buffer gas atoms. The latter energy, stored on the relative motion of the cylindrical parts of the peptide, will be responsible for the transformation of the peptide conformations as their potential barriers are overcome. The intraconversion of the two structures, driven by the thermal motion and the external electric field, will settle at a steady state close to equilibrium provided the field is weak.

The whole procedure depends on the ion–neutral interaction potential and the geometrical characteristics of the peptide, which can be estimated through reproduction of the experimental ion velocity or cross sections, eq 1, as a function of the gas temperature. One then can calculate the energy stored at the degrees of freedom of the peptide as well as second moments of the angular and velocity distribution functions as a function of gas temperature. We apply the present procedure in the case of an oligopeptide RA₁₅K (R is arginine, K is lysine, and A is alanine)⁵ and observe a complex behavior when rotation couples to vibration through the centrifugal interactions. The effect of the coupling, however, is diminished when $V(\varphi)$ is varied and the bending structures are trapped at relatively deep local potential minima. In this case, the population of the helix form, which emerges dominant at low temperatures, shifts toward a contracted form at high temperatures, in accordance to the results of ion mobility spectroscopy measurements.⁵

The performance of the method is examined for a specific peptide by varying the gas temperature but it can be used for the study of the dynamics of flexible peptides and macromolecules, which can be considered to vibrate along an effective (reaction) angular coordinate. Similarly, the electric field strength can be treated as an operational parameter and be used for the study of the behavior of the model system at strong fields and steady state conditions away from equilibrium. Extension to two or other vibration degrees of freedom is straightforward provided the equations of motion remain simple. In the case where the evolution equations become highly involved, the use of constraint dynamics methods has to be invoked.

METHOD

We consider a prototype model peptide that consists of two stiff helices connected by a flexible joint that can bend at the middle of the molecular body over an angle φ depending on an interaction potential $V(\varphi)$. The potential emerges primarily from the transformation of the flexible part of a macromolecule as φ is changing along a folding pathway.^{21,22} In some cases, the model is expected to apply effectively to a bending process, because during the peptide movement various conformation modes are getting excited and relaxed, but it is sufficient to consider only one dominant degree of freedom to reproduce the experimental results.^{7,23} Further, assuming the existence of a number of local minima in $V(\varphi)$, one would be able to reproduce the stabilization of a small number of structures observed at low temperature ion-mobility measurements. The corresponding heights of the barriers between the potential minima determine the rates of the conformational transformations. These features of the potentials are related to kinetic quantities obtained experimentally from analysis of the shifts of the ion-mobility spectroscopy peaks as the temperature is varied.⁷

Specifically, the prototype peptide consists of two identical rigid hollow cylindrical bodies connected to one another at a point of their circular edges. A section along the symmetry plane that includes the outer peptide body is presented in Figure 1. The derivation of the equations of motion of the

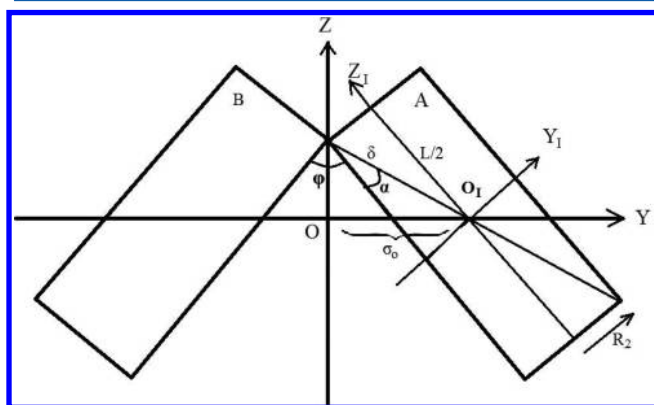


Figure 1. Body reference system, (X, Y, Z) , with center of axis, O , at the center of mass (CM) of the two-hollow-cylinder peptide model and local cylinder-A coordinate system, (X_1, Y_1, Z_1) , with center O_1 at the CM of cylinder A. The x -axes of both frames are pointing outward from the page of the figure. The geometrical parameters used for the cylinders are $R_1 = 2.5 \text{ \AA}$ (inner radius), $R_2 = 4.0 \text{ \AA}$ (outer radius), and $L = 8 \text{ \AA}$ for the length of the cylinder.

peptide degrees of freedom can be based on the kinetic energy expressed in Lagrangian form in terms of the velocities of the mass points of the peptide. The derivation of the kinetic energy expression is presented in the Supporting Information,

$$T = \frac{1}{2}m\mathbf{v}_0^2 + \frac{1}{2}(\mathbf{I}_{xx}\omega_x^2 + \mathbf{I}_{yy}\omega_y^2 + \mathbf{I}_{zz}\omega_z^2) + \frac{1}{2}\mathbf{I}_\varphi\dot{\varphi}^2 \quad (3)$$

where \mathbf{v}_0 is the inertial space velocity of the center of mass, m is the mass of the peptide, \mathbf{I}_{ii} are the moments of inertia about the body axes and \mathbf{I}_φ is the moment of inertia for the bending of the peptide,

$$\mathbf{I}_\varphi = \frac{1}{4}\left(2\mathbf{I}_{xx}^c + \delta^2 \cos^2\left(a + \frac{\varphi}{2}\right)m\right) \quad (4)$$

with $\delta = [(L/2)^2 + R_2^2]^{1/2}$ and a the angle between the diagonal and the height of the cylinder, Figure 1. The moments of inertia \mathbf{I}_{ii} are further expressed through the moments of a (single) hollow cylindrical rigid body about its symmetry axis, \mathbf{I}_{ii}^c ,

$$\begin{aligned} \mathbf{I}_{xx} &= 2\mathbf{I}_{xx}^c + m\sigma_0^2 \\ \mathbf{I}_{yy} &= 2\cos^2\frac{\varphi}{2}\mathbf{I}_{yy}^c + 2\sin^2\frac{\varphi}{2}\mathbf{I}_{zz}^c \\ \mathbf{I}_{zz} &= 2\cos^2\frac{\varphi}{2}\mathbf{I}_{zz}^c + 2\sin^2\frac{\varphi}{2}\mathbf{I}_{yy}^c + m\sigma_0^2 \end{aligned} \quad (5)$$

with $\sigma_0 = \delta \sin(a + \varphi/2)$. Finally, the moments of inertia of a hollow cylinder with the z -axis set along the cylinder main axis, Figure 1, are $\mathbf{I}_{xx}^c = \mathbf{I}_{yy}^c = (m_c/4)(R_1^2 + R_2^2 + (L^2/3))$ and $\mathbf{I}_{zz}^c = (m_c/2)(R_1^2 + R_2^2)$. The mass of a cylindrical body, m_c , is equal to $m/2$.

The form of the kinetic energy indicates that the motion of the peptide can be separated in the translational motion of the center of mass, the rotation, and an angular vibration. The translational motion requires the calculation of the total force in

the inertial frame acting on the mass center due to interaction with the gas atoms, $\sum_i \mathbf{F}_i$ and the action of the external homogeneous electrostatic field,

$$m\dot{\mathbf{v}}_0 = \sum_i \mathbf{F}_i + Ze\mathbf{E} \quad (6)$$

where Ze is the charge attached to the peptide and \mathbf{E} the electric field assumed in the z -direction. The rotation is followed through Euler equations in the body system,

$$\begin{aligned} \dot{L}_x + (\mathbf{I}_{zz} - \mathbf{I}_{yy})\omega_y\omega_z &= \tau_x \\ \dot{L}_y + (\mathbf{I}_{xx} - \mathbf{I}_{zz})\omega_z\omega_x &= \tau_y \\ \dot{L}_z + (\mathbf{I}_{yy} - \mathbf{I}_{xx})\omega_x\omega_y &= \tau_z \end{aligned} \quad (7)$$

with the torque $\boldsymbol{\tau}$, the angular momentum $\mathbf{L} = \mathbf{I}\boldsymbol{\omega}$, and the angular velocity $\boldsymbol{\omega}$, expressed in the body reference frame. We mention that the moments of inertia are varying in time, because they depend on the bending angle, eq 5. Torques may arise from the ion-atom interactions or the action of the external field. In addition, provision has been taken the external field to apply at appropriate different sites as the peptide folds or extends, because conformation changes may be accompanied by proton transfer between peptide residues.⁵

The kinetic equation of the angular vibration is obtained from Lagrange's equation with use of the kinetic energy from eq 3,

$$\begin{aligned} \ddot{\varphi}\mathbf{I}_\varphi - \frac{1}{16}\dot{\varphi}^2 m\delta^2 \sin(\varphi + 2\alpha) + \frac{1}{2}\sin\varphi(\omega_z^2 - \omega_y^2) \\ (\mathbf{I}_{zz}^c - \mathbf{I}_{yy}^c) - \frac{1}{4}m\delta^2 \sin(\varphi + 2a)(\omega_z^2 + \omega_x^2) \\ = F_\varphi \end{aligned} \quad (8)$$

where F_φ is the total force exerted on the cylindrical bodies having the tendency to modify the angle φ of the peptide. The internal potential $V(\varphi)$ contributes to the force, $F_\varphi = -(\partial V(\varphi)/\partial \varphi)$, along with the forces exerted by the gas atoms and possibly by the external field depending again on the position of the ion charges.

To express the mean force exerted on the peptide by the gas, we assume that the force is directed perpendicularly to the axis of each cylindrical body of the peptide toward the atom and is applied at a point located at a distance r_0 from this axis. At the flat sides of the cylinders the force is calculated as the sum of two contributions applied at the closest and the outermost distant points of the rim of the cylinder from the approaching atom. We have also taken provision for the atoms to be able to pass inside the hollow cylindrical bodies of the peptide with the forces acting as in the previous case, although the magnitude of the radius of the interactions r_0 and the form of the potential could prevent the atoms from entering inside the peptide body. However, the entrance of atoms inside the semirigid body of the model may not be accurately representing all actual cases. In some situations atoms with high kinetic energy may cross laterally a peptide and remain shorter time inside their body than in the present model where the particles always cross longitudinally the inner cylindrical body of the peptide. The scarcity of such energetic events in usual ion mobility spectrometry measurements favors the present approach.

The transport of ions under the action of an electrostatic field is reproduced efficiently through the use of two parallel MD simulation procedures, one for the gas atoms which remain

always at equilibrium, and one for the ions and images of atoms that undergo collisions with the ions. Specifically, via the first procedure (A procedure) the motion of gas atoms is simulated through an equilibrium microcanonical method without assuming interactions with the ions. In the second procedure (B procedure), however, the ions move independently from one another but interact with images of the gas atoms up to an interaction cutoff distance, R_{c1} . These images are generated at a distance, $R_{c2} > R_{c1}$, away from the ions on the basis of the positions of gas atoms of the A procedure. They are specific to each ion and are allowed to interact with the ion and to one another until they exit from the ion force field without further consideration. The approach works accurately at low density conditions where binary ion–neutral encounters take place; however, in moderately dense systems additional interactions need to be applied to the image atoms from (additional) atoms outside the interaction regions, so that they do not condense on the ion. In dense systems interactions are introduced specifically for each ion by atoms of the A procedure for some distance $R_{c3} > R_{c2}$, outside the ion–gas interaction region. Here, for the cutoffs $R_{c1} > R_{c2} > R_{c3}$ we use the values 3.2σ , 15.4σ , and 16.8σ with $\sigma = 2.556 \text{ \AA}$, the He collision diameter. The last cutoff, however, is obsolete at ideal gas conditions.

The equations of motion are integrated over a small time step with the use of the Gear predictor–corrector method,²⁴ PC, which involves three main calculation steps; a prediction step, where coordinates are predicted without evaluation of forces, a second evaluation step, where forces and torques are evaluated, and a third step, where prediction of new coordinates and other molecular quantities are calculated with use of the forces calculated in the second step. The molecular species are defined in space by three inertial coordinates, \mathbf{R} , representing the center of mass of the peptide, by a rotational matrix A characterizing the orientation and by the angle φ controlling the folding or extension of the peptide. The calculation approach of all the degrees of freedom is displayed schematically in Figure 2 where the inertial and the body coordinate systems are presented residing at different “places” connected by “bridges”. During the evaluation step forces and torques, \mathbf{F}^s and $\boldsymbol{\tau}^s$, are calculated initially at the inertial coordinate system and subsequently are transferred to the body system of Figure

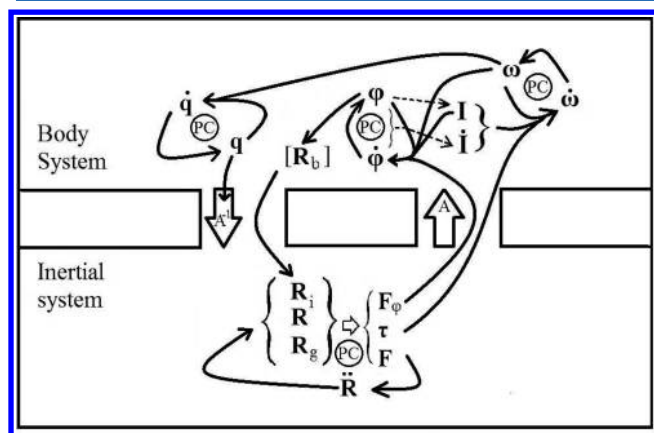


Figure 2. Schematic representation of the evaluation of variables during an integration (time) step of the equations of motion of a vibrating molecular system. The predictor–corrector procedure, denoted by (PC), acts at all evolving molecular coordinates and quaternions. From them derived quantities are obtained such as the moments of inertia and the rotational matrix, A .

1, \mathbf{F}^b and $\boldsymbol{\tau}^b$. This transformation is indicated by arrows that cross the right bridge in Figure 2 and is effected by the use of the rotation matrix A , which relates the inertial and body coordinates, $\mathbf{F}^b = A\mathbf{F}^s$ and $\boldsymbol{\tau}^b = A\boldsymbol{\tau}^s$. The opposite action in transforming body to inertial coordinates is utilized by the inverse matrix A^{-1} . The matrices are renewed at every time step of the procedure through the use of quaternions, $\mathbf{q} = \{q_0, q_1, q_2, q_3\}$, as intermediate quantities for the determination of the molecular rotation.²⁴ The quaternions also evolve in time through

$$\dot{\mathbf{q}} = \mathbf{M}\boldsymbol{\Omega} \quad (9)$$

$$\text{where } \boldsymbol{\Omega} = (0, \omega_x, \omega_y, \omega_z)^T \text{ and } \mathbf{M} = \frac{1}{2} \begin{pmatrix} q_0 & -q_1 & -q_2 & -q_3 \\ q_1 & q_0 & -q_3 & q_2 \\ q_2 & q_3 & q_0 & -q_1 \\ q_3 & -q_3 & q_1 & q_0 \end{pmatrix}$$

All the PC procedures are performed coherently, though information is transferred within the procedures during the intermediate evaluation step or at the end of a time step. One can follow the arrows starting from the calculation of forces in the inertial system, which are used for the calculation of the center of mass coordinates, \mathbf{R} , and the gas or image-gas coordinates, \mathbf{R}_g , directly through the PC procedure. The torques are transferred in the body system and are used for the evolution of the angular velocity, $\boldsymbol{\omega}$, and angle φ of the peptide, eqs 7 and 8. This calculation requires also the evaluation of the instantaneous moments of inertia of the ion, \mathbf{I} , and their rate of change, $\dot{\mathbf{I}}$. Further, the quaternions and the matrices A and A^{-1} are evaluated with the use of $\boldsymbol{\omega}$ as described above. In addition we follow three points, \mathbf{R}_b , that determine the molecular structure relative to the peptide mass center which are needed for the calculation of the ion-atom forces and their points of application. These sites are the point connecting the cylinders of the structure and the two mass centers of the cylinders. They depend on angle φ and are transformed in the inertial frame through $\mathbf{R}_i = A^{-1}\mathbf{R}_b$.

The MD simulation involves two parallel procedures as presented above, which are used to follow the motion of 108 gas atoms at ideal conditions of molar volume 0.02 m^3 (A procedure) and 130 independent ions (B procedure). The simulation is conducted in three stages. In the first stage, the atoms and the ions are forced to acquire certain mean properties for faster convergence to the final state. The gas is constrained at specific temperature and the peptide ions at certain effective temperatures parallel and perpendicular to the field, as well as, rotation and vibration temperatures. At weak electric fields the ion temperatures are well approximated by the gas temperature. In addition, at this stage the mean ion velocity is fixed close to the experimental value. At the second stage, gas atoms and ions are left without control of their mean values to relax to equilibrium and a steady drift state respectively, before accumulation of statistical properties starts at the last third stage. The duration of simulations is dictated by the relaxation time of the vibration which relaxes slower than the rest of the degrees of freedom of the ions. Efficient and low uncertainty results are obtained with a time step of 10^{-16} s . Due to the nonequilibrium state of the system, we monitor the evolution of the properties and extract mean values every $\delta t = 19.2 \times 10^6$ time steps. The first controlled stage was followed for $5\delta t$ time steps and the relaxation stage lasted for another $25\delta t$ steps. The calculation of statistical results including time

distributions were obtained during additional $30\delta t$ steps, which allowed several tenths of million ion–neutral encounters to occur. The electric field over the gas number density variable, E/N , has been set equal to 10 Td (1 Td = 10^{-21} V m²). This value is larger than the one used in ion mobility spectrometry but produces more ion–atom encounters during the molecular dynamics simulation and allows efficient calculation of properties without altering the results, because at such weak fields the mean velocity and other ion properties are expected to be independent of E/N .²⁵

With these provisions the ions maintain a steady drift motion and their trajectories can be employed for the study of the transport properties measured in drift tube experiments. The ion flux \mathbf{J} is well described by two contributions that characterize drift and diffusion

$$\mathbf{J} = n\mathbf{v}_d - \mathbf{D}\nabla n \quad (10)$$

where n is the ion number density, \mathbf{v}_d is the ion drift velocity in the direction of the field, and \mathbf{D} is a two-dimensional diagonal diffusion matrix with two independent components, a transverse one $D_{\perp} = D_{XX} = D_{YY}$ and a longitudinal one $D_{\parallel} = D_{ZZ}$. At low fields the two components approach each other and the diffusion coefficient becomes scalar quantity. The ion mobility is obtained from the mean velocity in the direction of the field, $\mathbf{v}_d = \langle \mathbf{v}_z \rangle$, through

$$K = \langle v_z \rangle / E \quad (11)$$

where E is the strength of the electric field. Further, effective temperatures are defined in perpendicular and parallel directions to the field through the mean kinetic energy components

$$\begin{aligned} \frac{1}{2}kT_X &= \frac{1}{2}m\langle (v_x - \langle v_x \rangle)^2 \rangle \\ \frac{1}{2}kT_Y &= \frac{1}{2}m\langle (v_y - \langle v_y \rangle)^2 \rangle \\ \frac{1}{2}kT_Z &= \frac{1}{2}m\langle (v_z - \langle v_z \rangle)^2 \rangle \end{aligned} \quad (12)$$

where m is the mass of the ion. The cylindrical symmetry of the ion motion due to the electric field sets $T_X = T_Y = T_{\perp}$ and $T_Z = T_{\parallel}$. Isotropy close to equilibrium requires $T_{\perp} = T_{\parallel}$. A total effective temperature can be determined for the translation through

$$\frac{3}{2}kT_{\text{eff}} = kT_{\perp} + \frac{1}{2}kT_{\parallel} \quad (13)$$

Similarly, effective temperature can be defined for the rotation,

$$T_r = \frac{1}{3}(T_{rx} + T_{ry} + T_{rz}) \quad (14)$$

with $T_{rx} = \frac{1}{2}\langle I_{XX} \rangle \langle (\omega_x - \langle \omega_x \rangle)^2 \rangle$, $T_{ry} = \frac{1}{2}\langle I_{YY} \rangle \langle (\omega_y - \langle \omega_y \rangle)^2 \rangle$, and $T_{rz} = \frac{1}{2}\langle I_{ZZ} \rangle \langle (\omega_z - \langle \omega_z \rangle)^2 \rangle$. In the case of vibration we express the kinetic energy through

$$\frac{3}{2}kT_{\text{vib}} = \frac{\langle (L_{\varphi} - \langle L_{\varphi} \rangle)^2 \rangle}{2\langle I_{\varphi} \rangle} \quad (15)$$

with $L_{\varphi} = I_{\varphi}\dot{\varphi}$, in analogy to the translational temperature. However, this is an indicative definition for the effective temperature because in systems where the internal degrees of freedom are coupled, as in the present case, the equipartition theorem does not apply.

Diffusion components can be calculated as time integrals of the velocity correlation functions,¹⁸ $C_{ii} = \langle (v_i(0) - \langle v_i(0) \rangle)(v_i(t) - \langle v_i(t) \rangle) \rangle$, with i representing $\{x, y, z\}$ directions,

$$D_{ii} = \int_0^{\infty} C_{ii}(t) dt \quad (16)$$

Because $C_{XX} = C_{YY}$, two independent diffusion components should appear, $D_{\perp} = (D_{XX} + D_{YY})/2$ and $D_{\parallel} = D_{ZZ}$. In addition, the MD simulation method can provide rates of the conformational change involving the folding of the peptide, as well as correlations between all the degrees of freedom. For later use, we have named the present program code MD2SF standing for molecular dynamics of two-state folding model.

APPLICATION

A. Interactions. Because the method can reproduce the motion of folding macromolecules, it can also be applied to systems that involve conformational changes, as well as other molecular transformations in drift tube experiments. Here, we apply the method to study the variation of ion transport and dynamics with respect to temperature for a designed peptide, RA₁₅K (R is arginine, K is lysine, and A is alanine), which has been studied experimentally.⁵ The dependence of the drift time distributions of this prototype peptide on the temperature has been explained with the consideration that the peptide ion undergoes a globule to helix transition at about 370 K. Further, as the temperature is raised above 400 K, a single peak remains in the distribution, which gradually shifts to positions where an extended globule ought to appear. The shift is attributed to gradual change of the residence times of the helix and globular forms of the peptide as effected by the available thermal agitation. The latter transition is best suited to be studied by our procedure, because the dynamics of the angular vibration can be followed efficiently by our nonequilibrium molecular dynamics method. However, because during the peptide transformation many degrees of freedom are involved, the process will only be represented effectively by a dominant angular vibration mode. We mention, in addition, that it has been suggested that the changes of the peptide structure are accompanied by proton transfer between arginine and lysine and therefore the force of the electric field has to be applied appropriately whenever the peptide structure changes.

Associating the two protein forms with bent structures, they can be introduced in the molecular model through consideration an angular potential, $V(\varphi)$, with functional form that consists of two potential minima and a barrier in between, as seen in Figure 3. The minima are introduced through two n - m model potentials, one with origin at $\alpha_1 = 0$ and the other at $\alpha_2 = \pi$,

$$V_{nm}^{(i)}(\varphi) = \frac{n\epsilon_i}{n-m} \left[\frac{m}{n} \left(\frac{\varphi_{m,i} - \alpha_i}{\varphi - \alpha_i} \right)^n - \left(\frac{\varphi_{m,i} - \alpha_i}{\varphi - \alpha_i} \right)^m \right] \quad (17)$$

with $i = 1, 2$. Here, we use $n = 4$ and $m = 2$, Table 1. We consider two local minima, one at small angle, $\varphi_{m,1} = 6^\circ$, and one at large angle, $\varphi_{m,2} = 170^\circ$, that represent the globule and helix forms. In addition, the shift of the time distribution peak from that of the helix to the one of the globule as the temperatures increases requires the helix (open structure) to be more stable and thus the potential minimum at large angles to be deeper. Initially, we have set $\epsilon_2 - \epsilon_1 = 5$ kcal mol⁻¹, Table 1.

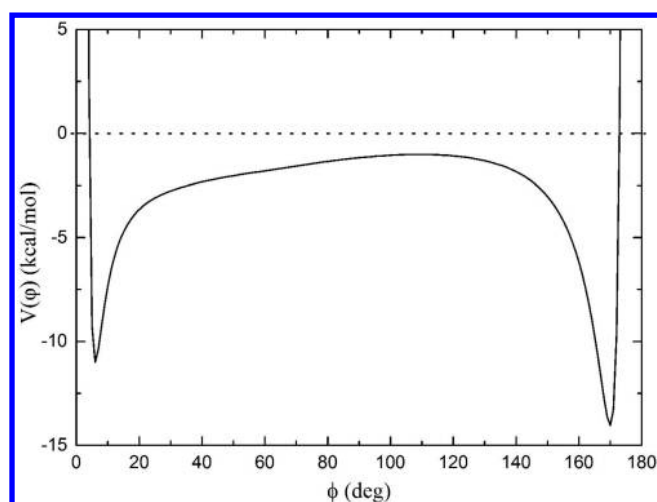


Figure 3. Angular model potential, $V(\varphi)$, for the folding of a flexible peptide.

Table 1. Potential Parameters

potential	φ_{m_j} or $\varphi_{o,i}$ (deg)	r_m (Å)	ϵ (kcal mol ⁻¹)	A (kcal mol ⁻¹)	σ (deg)
$V_{4,2}^{(1)}$	6		9		
$V_{4,2}^{(2)}$	170		14		
$V_G^{(1)}$	45			0.05984	10
$V_G^{(2)}$	20			-1.995	500
Ion-He		4.39	3.94		
He-He (LJ)		2.869	0.02030		

Additionally, the potential barrier has been shaped with the use of two gaussians ($i = 1, 2$),

$$V_G^{(i)}(\varphi) = A_i e^{-(\varphi - \varphi_{o,i})^2 / 2\sigma_i^2} \quad (18)$$

The overall potential presented in Figure 2 consists of the two contributions, eqs 17 and 18,

$$V_{nm}(\varphi) = \sum_{i=1,2} (V_{nm}^{(i)}(\varphi) + V_G^{(i)}(\varphi)) \quad (19)$$

Further, the ion-He interaction potential between the He atom and a cylinder of the peptide model was expressed through a 12-6-4 model potential

$$V(r) = \frac{\epsilon}{2} \left[\left(1 + \gamma\right) \left(\frac{r_m}{r}\right)^{12} - 4\gamma \left(\frac{r_m}{r}\right)^6 - 3(1 - \gamma) \left(\frac{r_m}{r}\right)^4 \right] \quad (20)$$

where r is directed perpendicularly to the axis of the cylindrical bodies of the peptide and ϵ and r_m are the depth and the position of the potential minimum. These potential parameters have been estimated through the reproduction of the ion velocity data, Figure 4, by a trial and error procedure and are reported in Table 1. The third parameter, $\gamma = 0.3258$, was obtained by matching the long-range limit with the correct form of the polarization interaction, $-\alpha_d/2r^4$,

$$V(r) = \frac{3\epsilon}{2} (1 - \gamma) \left(\frac{r_m}{r}\right)^4 = \frac{\epsilon^2 \alpha_d}{2r^4} \quad (21)$$

where α_d is the dipole polarizability of He, $\alpha_d = 1.3831a_0^3$.²⁶ The ion-atom mean force, $F_r = -dV(r)/dr$, is applied perpendicularly to cylinder axis at distance $r_0 = 1$ Å from the

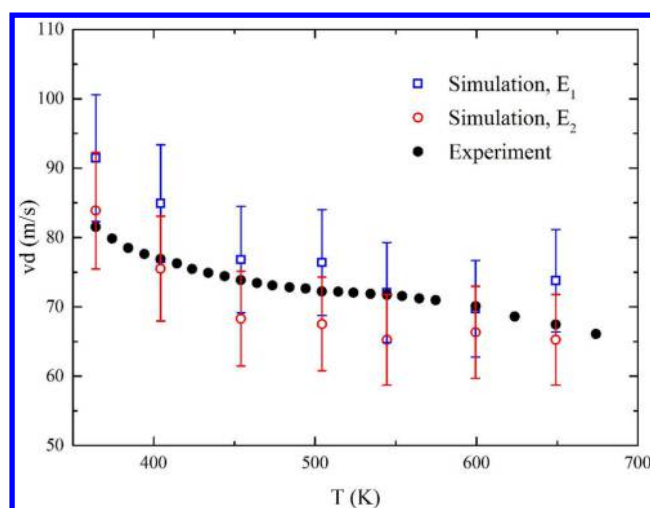


Figure 4. Experimental and calculated drift velocities of the protonated peptide $RA_{15}KH^+$ in He as a function of the gas temperature at $E/N = 10$ Td. E_1 represents $V(\varphi)$ potential with $\epsilon_2 = 14$ kcal/mol and E_2 represents $V(\varphi)$ potential with $\epsilon_2 = 34$ kcal/mol, both with $\pm 10\%$ error bars. The experimental data are estimated from the reported cross sections⁵ through eq 1.

axis. The radii of the hollow cylindrical bodies of the peptide are used for the moments of inertia, the inner and outer radii have been set $R_1 = 2.5$ Å and $R_2 = 4.0$ Å. In addition the length of the cylindrical bodies has been estimated from mobility tests to be $L = 8$ Å. The charge is positioned at one of the free ends of the cylindrical bodies of the peptide, though analysis of the protonation sites of the peptide indicates that the proton may be transferred from one end of the peptide to the other as globule converts to helix and vice versa.⁵ However, in both cases the geometry of the site where the electric field force is applied does not change with the charge transfer, allowing us to consider for simplicity the charge fixed at one end of the cylindrical bodies of the peptide. Tests of the use of a dynamically transferred charge whenever the φ -angle crosses the maximum of the barrier of $V(\varphi)$ have shown that there are no detectable variations on the simulation results as described below. Finally, the gas interactions are introduced through a Lennard-Jones He-He potential²⁷ that reproduces the properties of the gas at the experimental conditions very well, Table 1.

B. Results. With the appropriate equations of motion for the angular vibration, eq 8, and the peptide ion-atom model potential we can reproduce the mean motion and predict the dynamics of a flexible peptide ion such as $RA_{15}KH^+$. The calculated ion velocities are presented in Figure 4, together with velocities of the peptide ion which have been inferred through eq 1, with $E/N = 10$ Td, using the experimental cross section data obtained from ion-mobility spectrometry measurements.⁵ The reproduction of the drift velocity as a function of temperature has been used for the estimation of the ion-atom interaction potential parameters, ϵ and r_m of eq 20, as well as the structural model parameters. At low T values the ion mobility is more sensitive to the minimum of the ion-atom interaction potential though at high temperatures the repulsive part of the potential affects more drastically the ion motion. The obtained depth of the ion-atom interaction potential should be accurate within 10–20% and the position of the minimum within 5%. However, this estimate depends on the specific form of the angular potential and on the peptide structure that affects the results over the whole temperature

range. The angular potential affects the mean motion because it controls the contribution of the cross sections of the globule (contracted) and the helix (expanded) conformers to the scattering of the ions. In addition, the dimensions of the cylindrical bodies affect the ion–atom cross-section, though in a more uniform way with respect to the temperature.

With these reasonably accurate intermolecular interactions, we have calculated mean energies of all the ion and atom degrees of freedom. In Figure 5 we present the calculated mean

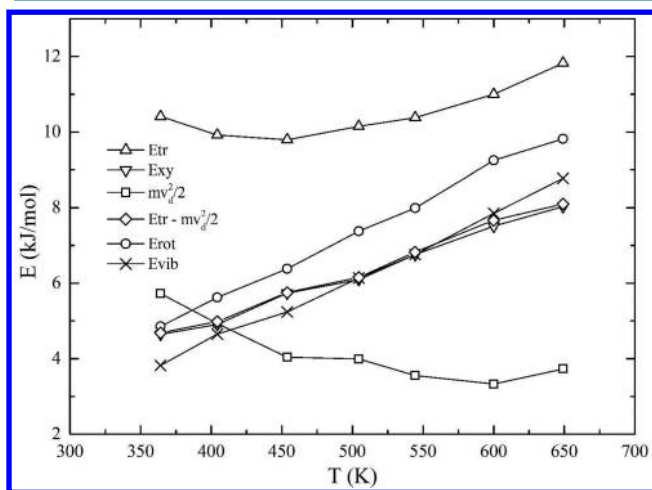


Figure 5. Mean ion kinetic energies E_{tr} , E_{xy} , E_{rot} and E_{vib} of (total) translation, translation transverse to the field, rotation, and vibration, respectively. The lowest curve is the kinetic energy of the ordered mean motion, shown as $mv_d^2/2$. The curve with diamonds has been obtained through the subtraction of the lowest curve from the upper one, E_{tr} .

kinetic energies of the ions as a function of the gas temperature. The components, translational transverse to the field, $3(E_x + E_y)/2$, rotational, E_{rot} and vibrational, E_{vib} , seem to approach each other within about $\pm 10\%$ difference. However, the (total) translation kinetic energy, E_{tr} , seems to deviate lying above the rest of the curves. This is due to the inclusion of the ordered kinetic energy due to the action of the electric field, presented with the lowest curve in Figure 5. The subtraction of this contribution from E_{tr} , produces a curve, indicated by $E_{tr} - mv_d^2/2$, which is consistent with the others.

The random energies expressed as effective temperatures for all the ion and atom degrees of freedom, through eqs 12–15, are presented in Figure 6. We observe that all the translational temperatures lie close to one another and all remain close to the gas temperature. At higher field strengths the situation is expected to differ, because during the ion flight field energy is stored differently in the motion parallel and perpendicular to the field. A similar situation is found when the effective temperatures of the translation, rotation, and vibration are compared with one another, Figure 6. In addition, the Wannier temperature,¹⁰ obtained through eq 2, seems to lie close to the translational temperature and to the rest of the internal temperatures as expected from a kinetic theory result. This coincidence is expected to hold for molecular ions with internal degrees of freedom in atomic gases and is quite appropriate for the description of the motion at weak fields.²⁸

Although the translation and rotation of the ions is found to behave as expected, the angular vibration seems to behave in a complex way. The mean angle of the peptide increases with

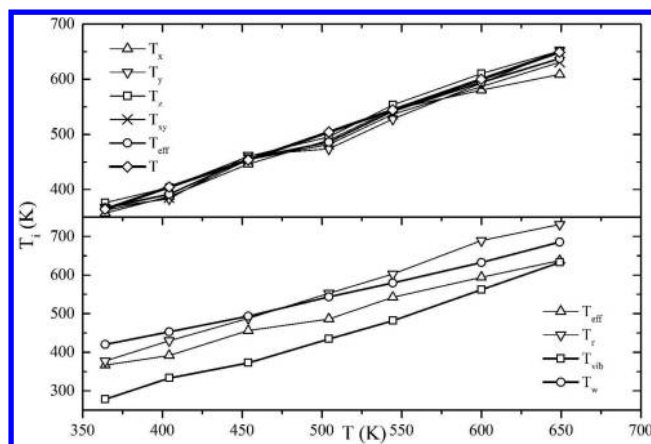


Figure 6. Comparison of effective translational temperature components, T_x , T_y , T_z , $T_{xy} = (T_x + T_y)/2$, and T_{eff} obtained from eq 13 and T is the gas temperature, upper panel. Effective temperatures for the translation T_{eff} , rotation T_{rot} , vibration T_{vib} and the Wannier temperature T_w , eq 2, lower panel.

temperature, Figure 7, starting from a quite low value at low temperature, although the angular potential acquires a deeper

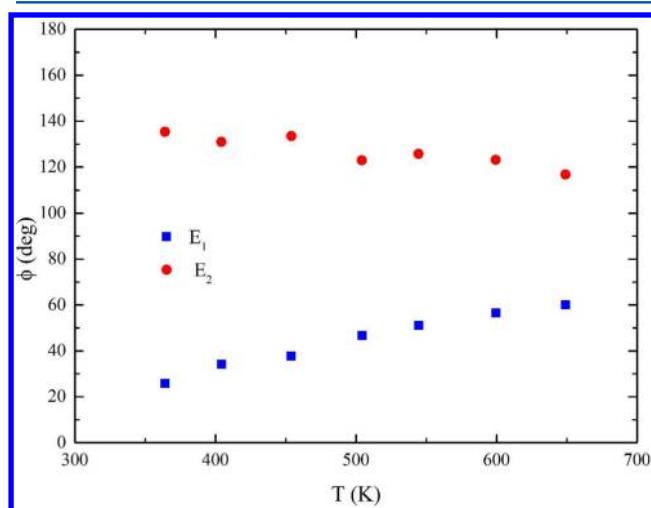


Figure 7. Mean bending angles as a function of temperature for potential $V(\varphi)$ with $\epsilon_2 = 14$ kcal/mol (E_1) and with $\epsilon_2 = 34$ kcal/mol (E_2).

potential minimum at 170° , Figure 3, and the opposite ought to appear. This behavior can be explained if one considers the role of the rotation in perturbing the motion of the angular vibration through the introduction of an effective angular potential. Specifically, the Hamiltonian of the rotation–vibration motion of a peptide ion based on the kinetic energy of eq 3 is

$$H = \frac{L_x^2}{2I_{xx}} + \frac{L_y^2}{2I_{yy}} + \frac{L_z^2}{2I_{zz}} + \frac{p_\varphi^2}{2I_\varphi} \quad (22)$$

where the numerators are squared angular and angular-vibration moments, $L = I\omega$ and $p_\varphi = I_\varphi\dot{\varphi}$. We can consider the rotation energy terms to act as effective potential, $V_e(\varphi)$, to the last angular vibration term. This potential is proportional to the inverse of the moments of inertia presented in Figure 8. Because the effective angular force $F_e = -dV_e(\varphi)/d\varphi$ depends on the slope of these curves, we observe that only the y

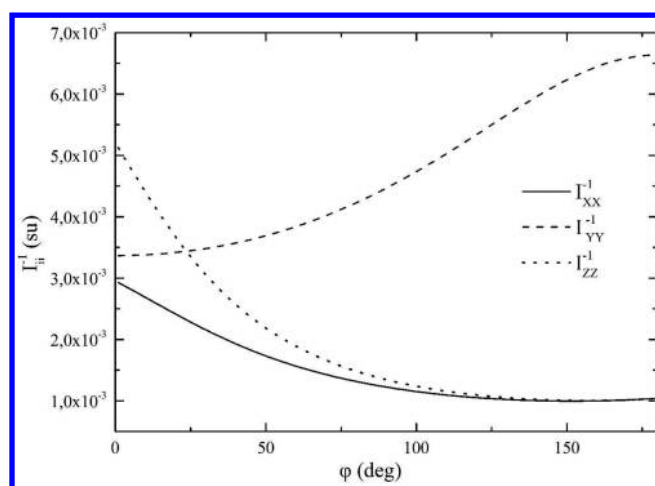


Figure 8. Inverse moments of inertia, in system units, proportional to the effective potential acting on the angular vibration.

component can produce a negative (contractive) force. This rotation axis is passing through the centers of symmetry of the two cylindrical bodies, Figure 1, and has the tendency to decrease the angle φ .

To examine the role of the rotational motion and the depth of the angular potential minimum at high φ values, we have deepened this local minimum and calculated the mean value of the bending angle at various temperatures, Table 2. We observe

Table 2. Mean Values of $\langle\varphi\rangle$ (deg) at Various Depths of the Potential Minimum ε_2 at $\varphi = 170^\circ$ and Two Gas Temperatures ($\varepsilon_1 = 9$ kcal/mol)

ε_2 (kcal/mol)	$T = 361$ K	$T = 600$ K
14	25.8	56.6
24	85	84.5
34	135	123
44	151	146

that indeed the model structure at low T can be trapped at high φ values provided the local potential depth becomes larger than 24 kcal/mol. This limiting value is sensitive to the rest of the molecular model parameters and can be varied with the structural parameters and the ion–atom interaction potential. To ensure the trap of the peptide ion at the helix form at low temperature, we have set $\varepsilon_2 = 34$ kcal/mol and performed molecular simulations for a number of gas temperatures. The experimental velocities⁵ are reproduced equally well with the shallow angular potential (low ε_2) within the accuracy of the calculation, Figure 4. Better agreement can be achieved through weakening of the peptide ion–gas potential interaction, because that would increase the ion mobility. We do not attempt this here because our aim is to study the general performance of the procedure in reproducing the dynamic behavior of the angular vibration of a flexible macromolecule with one bending mode. Further, the deepened angular potential produces mean angles that decrease with respect to the gas temperature, Figure 7, as expected due to the increase of the population of the contracted form with T . However, this decrease is weaker than the corresponding increase obtained for the initial angular potential. This indicates that the transfer of population out of the extended structure basin toward the contracted structure minimum is not fully developed at the present temperature

range. Increase of the slope of $\langle\varphi\rangle$ with respect to temperature can be obtained by decreasing the potential barrier between the angular potential minima. More generally, the relative population of the two stable structures will be dictated by the whole form of the angular potential and it may not lead to quantitative transfer of population from one structure to the other with variation of T . This case occurs often in peptide transformations and involves many structural changes at the residue level leading to transfer of the majority of the population from one state to another. Such population transfer can be implemented most easily in our procedure through consideration of effective angular potential that depends on temperature. Here, we do not employ such a potential, to avoid the introduction of additional empiricism in the molecular model.

Additional information about the frequency of the structure interchange is provided by the distribution of residence times of the model peptide to remain in the attractive basins of the angular potential. The potential basins that represent the two structures are defined by the position of the potential barrier, which resides at $\varphi = 110^\circ$. Thus, the contracted form has $0^\circ \leq \varphi \leq 110^\circ$ and the extended one $110^\circ \leq \varphi \leq 180^\circ$. We monitor the passage of the bending structures from the maximum of the potential and calculate the time they spent at each side of the barrier. The number of crossings, for the high ε_2 case during the last relaxed stage, is plotted in Figure 9, together with the

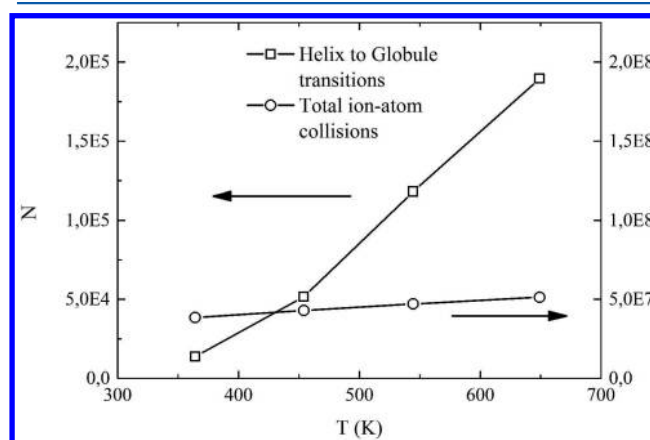


Figure 9. Number of helix to globule transitions and peptide ion–He encounters that emerge during similar MD simulations as a function of temperature.

number of peptide ion–atom collisions for comparison. We observe an almost linear dependence of the crossings on the temperature, with the structure interchange to vary faster with T than the ion–atom collisions. At low T , a small number of peptides have angular-vibration energy above the potential barrier and thus most of the peptides acquire extended form, whereas as the temperature increases and more peptides cross the barrier the number of contracted peptides increases. At these conditions the population of the structures involves peptides of trapped (extended or contracted) forms and energetic peptides that spend different time in extended or contracted forms. This time depends on the peptide vibration energy and the extension of the potential attractive basins.

We plot the residence times (per jump) of the peptide forms in Figure 10. The time distribution of the contracted structure appears to be wider but shorter than the extended one due to the form of the angular potential and the centrifugal forces

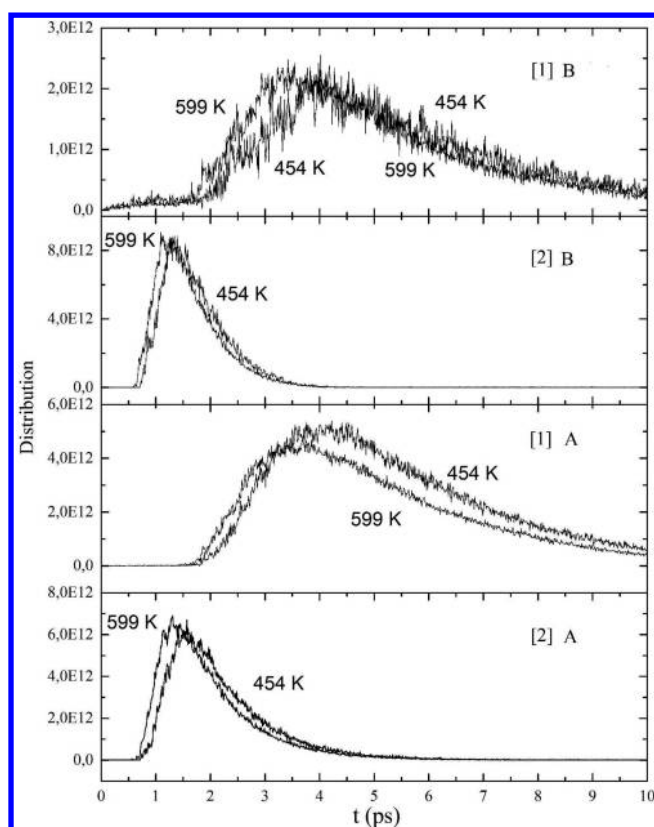


Figure 10. Distributions of residence times at two gas temperatures. [1] → (2) refers to the residence times at minimum [1] (small φ value), as the ions await to cross the barrier and move to minimum (2) (large φ -value), and vice versa for [2] → (1). Graphs indicated by A are produced with $\varepsilon_2 = 14 \text{ kcal mol}^{-1}$ and those by B with $\varepsilon_2 = 34 \text{ kcal mol}^{-1}$.

exerted on the ions. However, the increase of temperature shifts the distributions toward smaller values, because the ions move faster. In the case of shallow potential, $\varepsilon_2 = 14 \text{ kcal mol}^{-1}$, the peak of the distribution of the globule, [1]A, seems to decrease and that of the helix appears to increase, [2]A. This is in accordance with the shift of the mean angle of the peptide toward higher values with gas temperature, as seen in Figure 7. The opposite is obtained in the case of the deeper helix basin, $\varepsilon_2 = 34 \text{ kcal mol}^{-1}$, where the increase of the peak of the relevant residence time with T , [1]B, is in accordance with the shifts of population to the globule and the decrease of the mean angle value. We have also studied the dynamic transfer of the charge from one end of the peptide to the other as the ion was crossing the maximum of the potential, as suggested in the past.⁸ However, we did not obtain noticeable changes in the results, probably because of the similarity of the geometries of the two charged Λ -structures having the charge attached at different ends. Differences should occur in cases where the charge shifts between the joint of the two cylinders and one of the two ends of the peptide.

CONCLUSIONS

We have presented a nonequilibrium molecular dynamics method that reproduces the motion of a two-cylinder macromolecule model in a gas under the action of an electrostatic field. It is based on an approximation that treats the vibrating ion as consisting of two stiff hollow cylindrical bodies attached to each other. The whole molecular structure is

allowed to translate, rotate, and vibrate under the action of an electric field, an effective intramolecular angular potential and the ion–neutral gas interactions. The latter is represented by a 12-6-4 model potential that acquires accurate long-range polarization form. The proper equations of motion have been obtained from Lagrange's equation and have been implemented in the MD method of images of gas particles. The folding of a macromolecule is followed as an equilibrated unimolecular reaction that proceeds along an angular coordinate. This reaction coordinate crosses a potential barrier of an effective angular vibration potential as the peptide changes form.

The procedure is applied in the case of a peptide ion, RA_{15}K , that presents structural modifications with temperature in ion mobility spectroscopy measurements. Specifically, we have examined the shift of population of conformers between a globule and a helix structure with temperature, assuming an effective intramolecular potential with two local minima, one for the contracted and one for the extended peptide structure. Our mobility results reproduce the ion mobility spectrometry measurements within the calculation uncertainty but predict partial transformation of the helix peptides to extended globule ones and not transformation of the majority of the population as considered in the interpretation of the experimental data. The present procedure would require temperature dependent potentials to obtain such transfer from the extended to the globule form. We preferred to avoid the introduction of additional effectiveness into the two-cylinder model and we deferred the use of such angular potential to the near future.

The method is general and can be applied to other small or large flexible molecules and can be extended to systems with more vibration degrees of freedom, though the equations of motion may become quite complex. In such many-body flexible molecular systems constraint dynamics methods have to be implemented. The increase of the number of bending modes in the case of a general protein or a macromolecule makes difficult the implementation of the method because it requires determination of the position of bending modes and their folding potential, as well as, the ion–atom interactions. As the location of dominant bending modes may not be uniquely identified through ion mobility spectrometry measurements, theoretical methods should be invoked for their determination. The folding potentials depend on the nature of the bending modes and thus would have small transferability; however, the ion–atom interactions as representing a mean force should be more easily transferable. The direction of this mean force can still be assumed to be perpendicular to the axis of a specific body of a molecular system.

The method can also be implemented on a trial and error basis. Starting from a specific molecular model and considering a minimum of folding processes, one can produce results and compare them to experimental data until good agreement is obtained. On this basis, further improvements could be achieved depending on the number and nature of the foldings considered, as well as the suitability of the interaction potentials.

ASSOCIATED CONTENT

Supporting Information

The Supporting Information is available free of charge on the ACS Publications website at DOI: 10.1021/acs.jpca.5b05231.

Derivation of the kinetic energy of the peptide model, eq 3 (PDF)

■ AUTHOR INFORMATION

Corresponding Author

*A. D. Koutselos. Tel: +30-210-7274536. E-mail: akoutsel@chem.uoa.gr.

Notes

The authors declare no competing financial interest.

■ ACKNOWLEDGMENTS

The authors thank the Computer Center of the National and Kapodistrian University of Athens.

■ REFERENCES

- (1) Gidden, J.; Jackson, A. T.; Scrivens, J. H.; Bowers, M. T. Gas phase conformation of synthetic polymers: poly (methyl methacrylate) oligomers cationized by sodium ions. *Int. J. Mass Spectrom.* **1999**, *188*, 121–130.
- (2) Gidden, J.; Wyttenbach; Jackson, A. T.; Scrivens, J. H.; Bowers, M. T. Gas-phase conformations of synthetic polymers: poly(ethylene glycol), poly(propylene glycol), and poly(tetramethylene glycol). *J. Am. Chem. Soc.* **2000**, *122*, 4692–4699.
- (3) Hudgins, R. R.; Jarrold, M. F. Helix formation in unsolvated alanine-based peptides: helical monomers and helical dimers. *J. Am. Chem. Soc.* **1999**, *121*, 3494–3501.
- (4) Kaleta, D.; Jarrold, M. F. Helix-turn-helix motifs in unsolvated peptides. *J. Am. Chem. Soc.* **2003**, *125*, 7186–7187.
- (5) Kohtani, M.; Jones, T. C.; Sudha, R.; Jarrold, M. F. Proton transfer-induced conformational changes and melting in designed peptides in the gas phase. *J. Am. Chem. Soc.* **2006**, *128*, 7193–7197.
- (6) Jarrold, M. F. Helices and sheets in vacuo. *Phys. Chem. Chem. Phys.* **2007**, *9*, 1659–1671.
- (7) Zilch, L. W.; Kaleta, D. T.; Kohtani, M.; Krishnan, R.; Jarrold, M. F. Folding and unfolding of helix-turn-helix motifs in the gas phase. *J. Am. Soc. Mass Spectrom.* **2007**, *18*, 1239–1248.
- (8) Kohtani, M.; Schneider, J. E.; Jones, T. C.; Jarrold, M. F. The mobile proton in polyalanine peptides. *J. Am. Chem. Soc.* **2004**, *126*, 16981–16987.
- (9) Mason, E. A.; McDaniel, E. W. *Transport Properties of Ions in Gases*; Wiley: New York, 1988; p 276.
- (10) Wannier, G. H. Motion of gaseous ions in strong electrostatic fields. *Bell Syst. Tech. J.* **1953**, *32*, 170–254.
- (11) Mesleh, M. F.; Hunter, J. M.; Shvartsburg, A. A.; Schatz, G. C.; Jarrold, M. F. Structural Information from Ion Mobility Measurements: Effects of the Long-Range Potential. *J. Phys. Chem.* **1996**, *100*, 16082–16086.
- (12) Shvartsburg, A. A.; Mashkevich, S. V.; Baker, E. S.; Smith, R. D. Optimization algorithms for ion mobility calculations. *J. Phys. Chem. A* **2007**, *111*, 2002–2010.
- (13) Shvartsburg, A. A.; Mashkevich, S. V.; Michael Siu, K. W. Incorporation of thermal rotation of drifting ions into mobility calculations: drastic effect for heavier buffer gases. *J. Phys. Chem. A* **2000**, *104*, 9448–9453.
- (14) Book, L. D.; Xu, C.; Scuseria, G. E. Carbon cluster ion drift mobilities. The importance of geometry and vibrational effects. *Chem. Phys. Lett.* **1994**, *222*, 281–286.
- (15) Koutselos, A. D. Molecular dynamics simulation of gaseous ion-motion in electrostatic fields. *J. Chem. Phys.* **1995**, *102*, 7216–7220.
- (16) Balla, G.; Koutselos, A. D. Molecular dynamics simulation of ion transport in moderately dense gases in an electrostatic field. *J. Chem. Phys.* **2003**, *119*, 11374–11379.
- (17) Koutselos, A. D. Mixed quantum-classical molecular dynamics simulation of vibrational relaxation of ions in an electrostatic field. *J. Chem. Phys.* **2006**, *125*, 244304–244311.
- (18) Koutselos, A. D. Transport and dynamics of $O_2^+(X^2\Pi_g)$ in Kr under the action of an electrostatic field: Single or multiple potential energy surface treatment. *J. Chem. Phys.* **2011**, *134*, 194301–194307.
- (19) Chen, X.; Thachuck, M. Collision-induced alignment of H_2O^+ drifting in helium. *J. Chem. Phys.* **2006**, *124*, 174501–174508.
- (20) Linse, P.; Palencar, P.; Bleha, T. A new two-state polymer folding model and its application to α -helical polyalanine. *J. Phys. Chem. B* **2011**, *115*, 11448–11454.
- (21) Kortvelyesi, T.; Stacho, L. L.; Domotor, Gy.; Jojart, B.; Ban, M. I. Pathway of the conformational transitions in flexible molecules. *J. Mol. Struct.: THEOCHEM* **2005**, *725*, 145.
- (22) Brancolini, G.; Venturini, A.; Zerbetto, F. Potential energy surface and kinetics of the helix-coil transition in a 33-peptide. *Theor. Chem. Acc.* **2007**, *118*, 25–34.
- (23) Sudha, R.; Kohtani, M.; Jarrold, M. F. Non-covalent interactions between unsolvated peptides: helical complexes based on acid-base interactions. *J. Phys. Chem. B* **2005**, *109*, 6442–6447.
- (24) Allen, M. P.; Tildesley, D. L. *Computer Simulation of Liquids*; Clarendon Press: Oxford, U.K., 1987.
- (25) Mason, E. A.; McDaniel, E. W. *Transport Properties of Ions in Gases*; Wiley: New York, 1988; p 140.
- (26) Thakkar, A. J. The generator coordinate method applied to variational perturbation theory. Multipole polarizabilities, spectral sums, and dispersion coefficients for helium. *J. Chem. Phys.* **1981**, *75*, 4496–4501.
- (27) Hirschfelder, J. O.; Curtiss, C. F. *Molecular Theory of Gases and Liquids*; John Wiley: New York, 1964; Appendix I.
- (28) Viehland, L. A.; Lin, S. L.; Mason, E. A. Kinetic theory of drift-tube experiments with polyatomic species. *Chem. Phys.* **1981**, *54*, 341–364.